J. Electrochem. Sci. Eng. **11(3)** (2021) 143-159; http://dx.doi.org/10.5599/jese.956

Open Access: ISSN 1847-9286
www.jESE-online.org

Original scientific paper

Determination of 4-nitrophenol using MoO_3 loaded glassy carbon electrode *via* electrochemical sensing approach

Bhagyashri B. Kamble[1], Kalyanrao M. Garadkar[2], Kirankumar K. Sharma[3], Pravin Kamble[3], Shivaji N. Tayade[2] and Balu D. Ajalkar[1,✉]

[1]*Shivraj College, Gadhinglaj, Shivaji University, Kolhapur Maharashtra, India 416502*
[2]*Department of Chemistry, Shivaji University, Kolhapur, Maharashtra, India 416004*
[3]*School of Nanoscience and Technology, Shivaji University, Kolhapur, Maharashtra, India 416004*

Corresponding author: ✉bajalkar@rediffmail.com; Tel.: +91- 9404255274

Received: January 27, 2021; Revised: April 14, 2021; Accepted: April 18, 2021; Published May 24, 2021

Abstract

In order to raise possible ways of MoO_3 synthesis and improve its existing applications, MoO_3 nanomaterial was successfully synthesized through the solvo-hydrothermal route by utilizing a mixture of ionic liquid (1-butyl-3-methylimidazolium bromide) as a solvent, and water as co-solvent in 1:1 ratio. The morphology and structural parameters of IL-assisted MoO_3 product were examined by X-ray diffraction (XRD), Fourier-transform infrared spectroscopy (FT-IR), and scanning electron microscopy (SEM). Additionally, the surface wettability and particle size distribution were inspected using the contact angle and dynamic light scattering (DLS) analysis. Glassy carbon electrode (GCE) surface was then modified by IL-assisted MoO_3. The formed IL-MoO_3/GCE was employed as an electrochemical sensor for determination of 4-nitrophenol (4-NP), which is very toxic and important pollutant. The redox behavior of 4-NP at the surface of IL-MoO_3/GCE was investigated by cyclic voltammetry (CV) and differential pulse voltammetry (DPV) techniques. Limits of detection (LOD) and limits of quantification (LOQ) determined from CV were found to be 6.76 and 22.5 μM, while from DPV recordings, 5.41 and 18.0 μM are found. The obtained results clearly reveal possible application of MoO_3 for selective and sensitive sensing of 4-NP. The decorated electrode was successfully employed for determination of 4-NP in the river water real samples.

Keywords

Molybdenium oxide nanoparticles; ionic liquid; solvo-hydrothermal synthesis; nitrophenol; voltammetry techniques

Introduction

Environmental crisis across the globe has been increasing day by day due to numerous causes such as global warming, ozone depletion, and the greenhouse effect. High contribution to the extensive environmental pollution is caused by the exponential growth of industrialization, which frequently uses different hazardous starting materials. A good example of hazardous materials is 4-nitrophenol (4-NP) that has been used as a starting material in pesticide production and manufacturing of drugs and dyes. Consequently, 4-NP has been frequently found in wastewaters from pharmaceutical, paint, and petrochemical industries.

Environmental exposure and distribution of 4-NP in air, water, residue, and soil were found out to be 0.006, 94.6, 4.44 and 0.95 %, respectively. These data suggest that an enormous amount of 4-NP is released in the environment, particularly water, in which even after degradation, it retains for almost 2.8 to 13.7 days [1,2]. Consequently, 4-NP is considered as the major pollutant by EPA (Environmental protection agency), USA. Several studies showed that 4-NP is potentially genotoxic and considered as drug impurity with the threshold limit value (TLV) of 4 mg/day for humans, which is relatively higher than the reference dose [3]. Therefore 4-NP is considered as a hazardous compound which leads to unfavorable effects on human health such as nausea, cyanosis, *etc.* 4-NP is highly stable and soluble in water and therefore, purification of water by conventional methods such as adsorption, extraction, and nanofiltration is a challenging task since these methods involve formation of toxic byproducts [4]. Because of these negative impacts, the need for detection and monitoring of concentrations of 4-NP has become the priority of researchers. It has generally been considered essential to develop a relatively inexpensive and simple method for rapid detection of 4-NP in an aqueous solution, with high sensitivity and selectivity.

Different techniques have been utilized for determination of 4-NP, such as spectrophotometric method [5,6] high-performance liquid chromatography [7,8] high-performance capillary electrophoresis [9], and gas chromatography [10]. The main disadvantages of these methods, however, are complexity, cost, and time-consuming. Nowadays, electrochemical methods have established significant attention due to their immense advantages such as good sensitivity, fast response, and simple operation [11,12].

It has already been observed, however, that electrochemical detection of 4-NP at bare electrodes is seriously suffering from high over-potential, interference issues, and low sensitivity. Therefore, electrode surfaces were usually chemically modified, and extensively used to develop highly efficient electrochemical sensors for determination of 4-NP. In the past decade, numerous studies on the use of electrodes chemically modified with metal nanoparticles [13,14] metal oxide nanoparticles [15], graphene oxide [16], graphene-gold nanoparticles and their nano-composites have been reported to detect and measure 4-NP. Among these materials, graphene and its derivatives have been preferably studied in electrochemical sensing due to their superior properties such as two-dimensional layered structure, low charge transfer resistance, and wide electrochemical potential window [17]. However, graphene consists of zero band gaps that limit its diverse applications.

During the past decade, various metal oxides (*e.g*. Mn, Cu, Co, Ti, Mo, and W) and their electrode materials have turn out to be an essential part of the research field concerned primarily to avoiding environmental and energy crises *via* degrading environmental organic pollutants and green energy production [18]. It is interesting to note, however, that two-dimensional structure of MoO_3, is analogous to graphene, and therefore, it could also be considered as a promising material in sensing applications, due to high surface area, thermal stability, superior mobility, and high electrochemical performances compared to other metal oxides [19].

MoO_3 is made up of MoO_6 layers, and each layer is held together by strong covalent bonds and weak Van der Waals force with a wide band-gap (3.0 eV) [20]. These structural properties of MoO_3 can offer a diverse approach in the field of electrochemical sensing. Thus, MoO_3 has been studied for efficient bio-sensing (glucose and dopamine) due to its structure and bonding between Mo-O, leading to the intercalation of analyte. Various stoichiometric and reduced forms of molybdenum oxide (MoO_x) have been explored in dye degradation and other applications such as Li-ion batteries and supercapacitors [21]. Consequently, MoO_3 is the most studied, environment-friendly, low-cost electrode material in the energy storage field, what is due to its significant multiple oxidation states, which could promote redox reaction of electrode. Therefore, MoO_3 is generally considered as an appreciable electro-active compound [22,23].

Various synthetic routes of MoO_3 have already been studied, such as chemical bath deposition [24], sol-gel [25] and hydrothermal methods [26] among which, the hydrothermal is the simplest and cheapest method. In this work, the hydrothermal route is explored in preparation of MoO_3 using ionic liquid (IL). IL has been considered as a designer solvent due to its organized structure with extended hydrogen bonds, which exhibit exclusive interaction with metal nanoparticles. Therefore, many efforts have already been reported to study the interaction between some ionic liquids and metal nanoparticles [27,28].

Herein, we report a facile synthesis of MoO_3 using IL, $[BMIM]^+[Br]^-$, as co-solvent to achieve different morphology and better performance of MoO_3. IL assisted synthesized MoO_3 was then used to modify GCE and prepare IL-MoO_3/GCE, which was subsequently tested as an electrochemical sensor for determination of 4-NP. For the electrochemical sensing analysis, cyclic voltammetry (CV) and differential pulse voltammetry (DPV) techniques were employed.

Experimental

Chemicals

4-nitrophenol (≥90 %), n-butyl bromide (C_4H_9Br) and toluene ($C_6H_5.CH_3$) (AR) (≥99 %) were procured from Thomas Baker Chemicals, Mumbai, India, while 1-methylimidazole ($C_4H_6N_2$) (≥99 %) was obtained from Spectrochem Pvt. Ltd. Mumbai, India. Ammonium heptamolybdate tetrahydrate (AHM) (99 % pure) ($(NH_4)_6Mo_7O_{24}$ $4H_2O$), concentrated nitric acid (HNO_3) (≥99 %), absolute ethanol (≥99 %), dihydrogen potassium orthophosphate (KH_2PO_4) (≥99 %), and dipotassium orthophosphate (K_2HPO_4) (≥99 %) were obtained from S D Fine-Chem. Ltd., Mumbai, India.

Synthesis of ionic liquid assisted MoO_3

MoO_3 was synthesized by solvo-hydrothermal route using a mixture of IL, $[BMIM]^+$ $[Br]^-$, and triple distilled water (TDW) in 1:1 ratio as reported in our previous work [29]. Ammonium heptamolybdate (0.03 M) was initially dissolved in a mixture of IL. After dissolution, the concentrated HNO_3 was added to the same beaker with strong stirring. The above solution was moved into Teflon-lined stainless-steel autoclave containing a previously cleaned glass substrate. The hydrothermal reaction was carried out at the temperature of 180 °C for 6 h. After completion of the reaction, the autoclave was naturally cooled to room temperature. Deposited MoO_3 thin film was washed few times with TDW, ethanol, and dried at 60 °C. Annealing process of dried MoO_3 thin film was carried out at 350 °C for 2 h. The annealed MoO_3 was used for fabrication of GCE for electrochemical analysis. The mechanism of reaction is represented by equations 1-4 and the experimental setup is shown in Scheme 1.

$$[Bmim]^+ [Br]^- + H_2O \rightarrow \text{IL mixture} \quad (1)$$

$$\text{IL mixture} + [(NH_4)_6Mo_7O_{24}.4H_2O] \rightarrow 6[Bmim]^+ [Mo_7O_{24}]^{-6} + 6NH_4Br \quad (2)$$

$$6[Bmim]^+ [Mo_7O_{24}]^{-6} + 6NH_4Br + 6HNO_3 \rightarrow 6[Bmim]^+ [Br]^- + 6NH_4NO_3 + [H_6Mo_7O_{24}] \quad (3)$$

$$[H_6Mo_7O_{24}] \rightarrow 7MoO_3 + 3H_2O \quad (4)$$

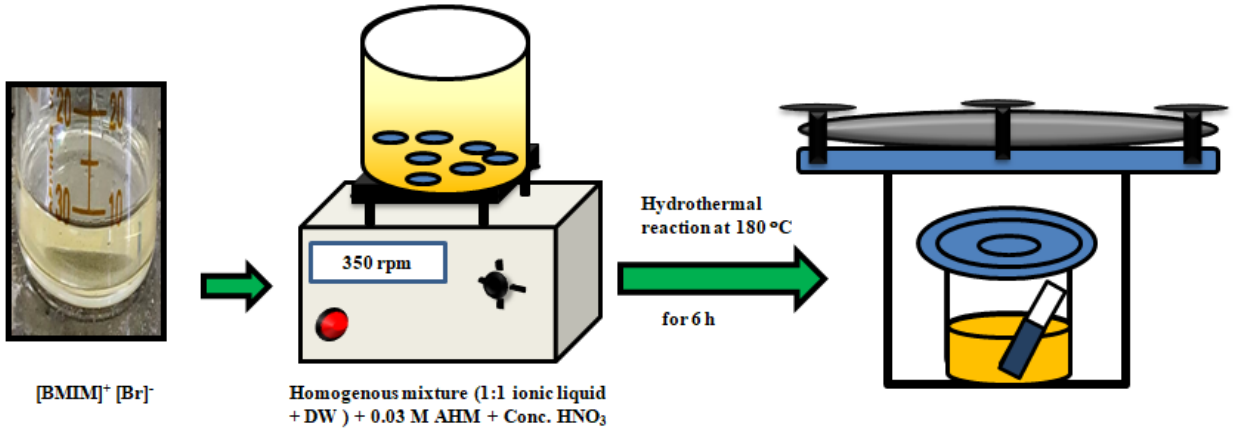

Scheme 1. *Hydrothermal reaction setup for IL-assisted synthesis of MoO_3 thin film*

Preparation of modified electrode

IL assisted MoO_3 film was dispersed in ethanol (2 mg mL^{-1}) with the aid of ultrasonication for 30 minutes. GCE surface was cleaned by polishing with Al_2O_3 (0.05 µm) using a polishing cloth, then washed several times with distilled water, ultrasonicated for 5 minutes, and finally dried. 2 µL of MoO_3/ethanol dispersion was drop coated on pre-cleaned GCE, until GCE surface was exclusively covered by MoO_3 particles. To provide stability of deposited MoO_3 particles, Nafion 2 %, perfluoro-sulfonated polymer was added. The active surface area of the modified GCE was determined using 1 mM ferrocene, a standard redox couple in 0.1M KCl as the supporting electrolyte at room temperature, and Randles–Ševčik equation. For a reversible redox process, the peak current is expressed as

$$i_p = 2.69 \times 10^5 n^{3/2} A D_{app}^{1/2} C_o v^{1/2} \quad (5)$$

where i_p represents anodic peak current, n = 1 is number of electrons transferred, A is active surface area of electrode, $D_{app} = 0.16 \times 10^{-6}$ cm^2 s^{-1} is diffusion coefficient of ferrocene [30], v is potential scan rate and C_o is bulk concentration of ferrocene (1 mM). The active surface area of the modified electrode is determined as 0.54 cm^2, which is about 7 times greater than the geometric area (0.0707 cm^2) of bare GCE. The roughness factor was found to be 7.22, when calculated from the ratio of active surface area to the geometric area of the working electrode.

Characterizations

Powder X-ray diffraction (XRD) was recorded using (Thermo ARL X'TRA with Cu*K*α irradiation, λ = 0.154056 nm). The scanning electron microscopy (SEM) observation was performed with Hitachi SU-70 (Japan). Fourier transform infrared (FT-IR) spectroscopy analysis was performed using FT-IR--6600 spectrometer (Bruker Company), the contact angle determination was performed using Holmarc opto mechanics with 10 microliter droplet, and DLS analysis was employed using Litesizer-500.

Electrochemical experiments

The redox behavior of 4-NP was examined using cyclic voltammetry (CV), differential pulse voltammetry (DPV) techniques and electrochemical workstation (PGATAT302N Metrohm Auotolab). A three-electrode system was employed, where either bare or modified GCE served as the working electrode (geometric area = 0.07 cm^2), a platinum wire as the counter electrode, and Ag/AgCl-3 M KCl as the reference electrode. Cyclic voltammetry was recorded in the potential range from −0.2 to 0.6 V, with 4-NP in phosphate buffer solution of pH 5.8. A differential pulse voltammetry was conducted in the

range of −0.2 to 0.6 V, with modulated amplitude 0.025 V, step width of 0.005 V, and interval time of 0.5 s. Electrochemical impedance spectroscopy (EIS) measurements were performed in 0.1 M KCl solution containing 1 mM ferrocene with frequencies ranging from 10^5 to 0.1 Hz, and AC amplitude of the applied wave potential of 10 mV. EIS measurements of bare and modified electrodes were performed at 0.15 V.

Results and discussion

Structural studies of IL-MoO_3

Figure 1 depicts highly intense and spiky diffraction peaks at 2θ = 12.60, 23.26, 25.70, 27·34, 33.89, 38·96, 46.06, 49.18, 52.80, 58.66 and 64.60°, corresponding to the planes (020), (110), (021), (111), (150), (002) (211), (081) and (062), indicating orthorhombic crystal structure. All XRD peaks were recognized as MoO_3 peaks from JCPDS card 76-1003 [31].

The intense and sharp peaks from XRD imply that the prepared material is of crystalline nature. The calculated lattice constant of annealed MoO_3 was found as: *a* = 3.94 Å, *b*=14.01 Å and *c* = 3.70 Å, which were in good agreement with the JCPDS card for orthorhombic structure. The crystallite size and shape in finely divided powdered solid often help to associate many physical properties of the system. The average crystallite size of 62.8 nm was anticipated from Debye-Scherrer's equation

$$D = \frac{0.9\lambda}{\beta \cos\theta} \quad (6)$$

where *D* is average crystallite size, λ = wavelength, θ = diffraction angle, and β = FWHM (full width half maximum).

FTIR study of IL-MoO_3

Figure 2 shows FT-IR spectrum of as-synthesized IL-MoO_3. Different peaks appear at 617 to 3392 cm^{-1}. The bending vibration mode of Mo-O-Mo appears at 617 cm^{-1}, while vibrations of Mo-O-Mo of Mo^{6+} are attributed by 870 cm^{-1} [32].

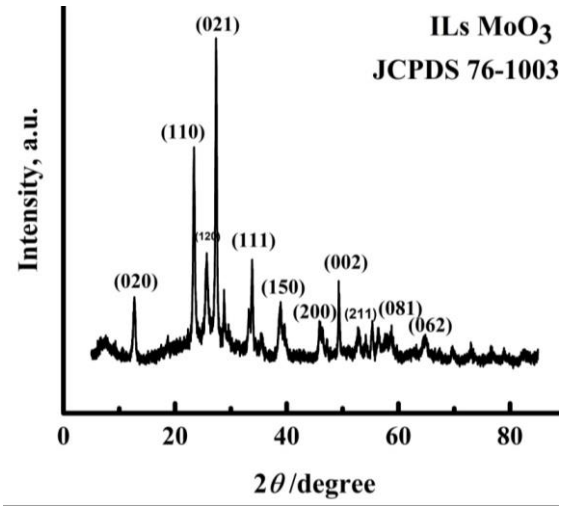

Figure 1. *XRD pattern of IL-MoO_3*

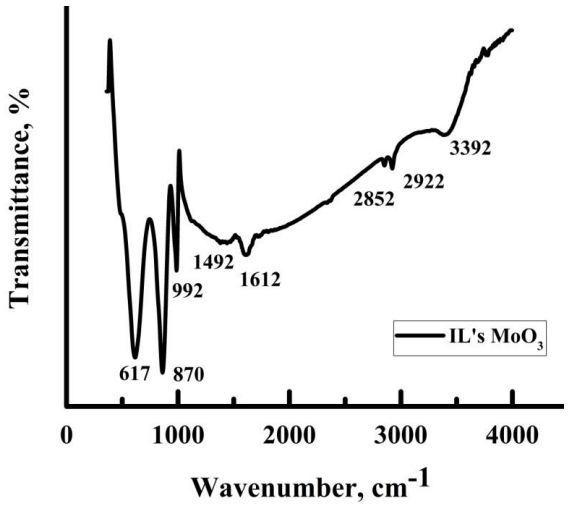

Figure 2. *FT-IR spectrum of IL-MoO_3*

The characteristic peak of Mo-O-Mo is slightly shifted to a higher wavelength, what indicates the peculiar structure of MoO_3 obtained in the presence of IL. The absorption band at 992 cm^{-1} is assigned to the presence of a Mo=O bond [33]. Therefore, the absorption peaks below 1000 cm^{-1} are associated to the interatomic vibration of metal and oxygen. The peak appearing at 1492 cm^{-1} and 2852-2922 cm^{-1} are associated with imidazole H-C-C and H-C-N bending mode [34]. The

characteristic absorption band of the hydrogen-bonded hydroxyl group (-OH) appears at 3392 cm^{-1} (ν-OH) and 1612 cm^{-1} (δ-OH). Therefore, FT-IR results show the successful formation of IL-MoO_3.

Morphology of IL-MoO_3 (SEM)

Figure 3 shows SEM images of IL-MoO_3, revealing an aggregated, irregular and to some extent, a flower-like morphology.

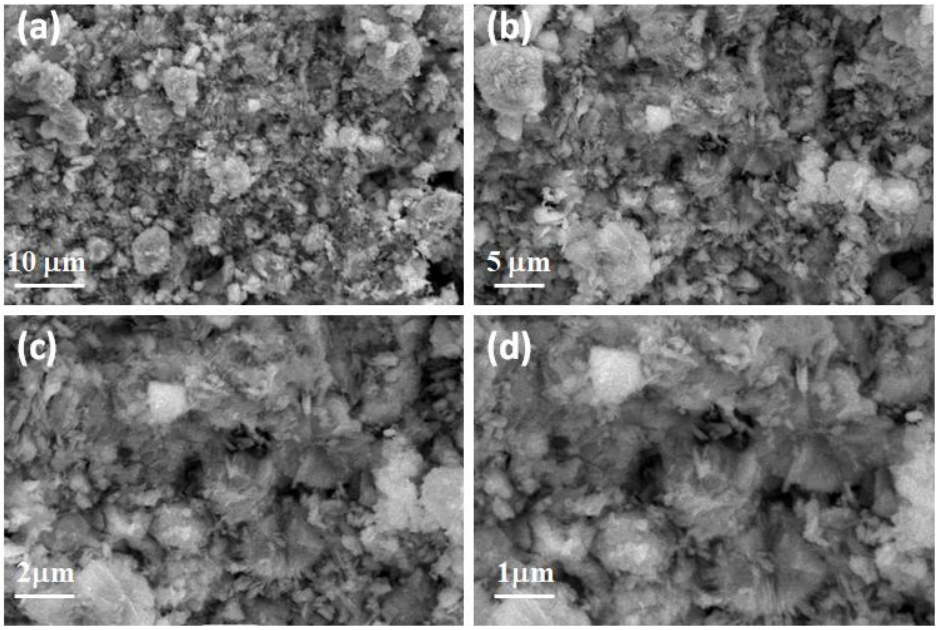

Figure 3. *SEM images of IL-MoO_3 at different resolutions from (a) to (d)*

It is well known that the cationic part of IL $[BMIM]^+[Br]^-$, can form micelles in the aqueous solution which further promote aggregation [35]. During formation of MoO_3, IL is consumed as co-solvent, and the resulting increase in the steric hindrance and growing alkyl chain lengths limits diffusion of Mo^{6+} ions and hence, the aggregated particles are developed. IL moiety consists of hydrogen bond and free ions, which induce electrostatic interaction and Van der Waals force into metal nanoparticles. IL typically interacts with the surface of metal nanoparticles with either cations or anions to produce diversity in morphology. It is also well known that the anion dominant interaction shows flower shape morphology [36].

Scheme 2 indicates that bromine anions prefer to adsorb on the surface of metal oxide nanoparticles along with the imidazole moiety to form hydrogen bond, leading to enhancement of electrostatic interaction to induce flower-like morphology.

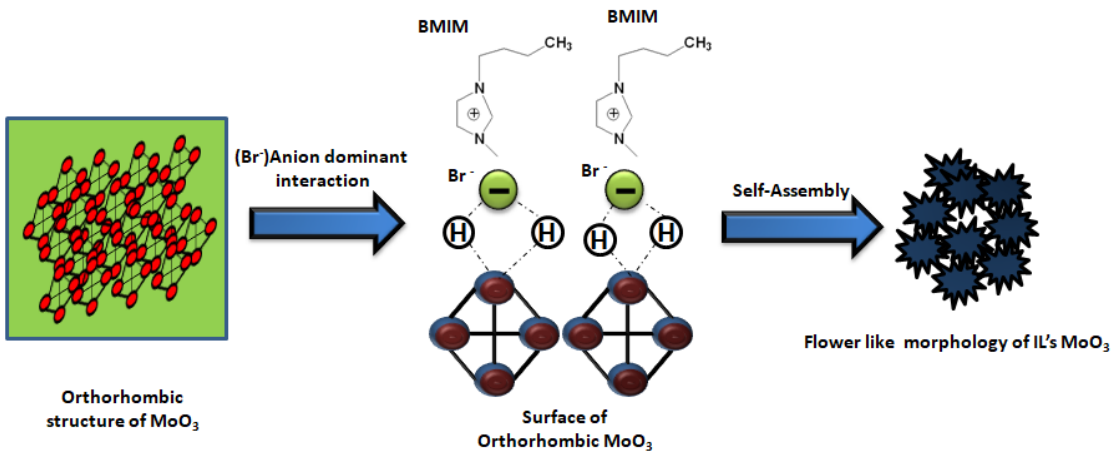

Scheme 2. *Ionic liquid $[BMIM]^+[Br]^-$ and metal oxide surface interaction*

Contact angle measurement of IL-MoO_3

The measurement of the contact angle of IL-MoO_3 on the surface of the glass substrate was performed using *Sessile drop method*. The contact angle is a major factor for characterization of surface wettability and also, measurements of phase interface on the solid surface. If the contact angle is smaller than 90°, the solid surface is considered hydrophilic and if the contact angle is larger than 90°, the surface is referred as hydrophobic [37]. As shown in Figure 4, the contact angle of water at the surface of IL-MoO_3 is ~67.3°. Since the contact angle is less than 90°, there is an increase in the hydrophilicity of IL-MoO_3, what can influence the buffer solution. As a result, IL-MoO_3 surface shows compatibility for immobilization of analyte [38]. Therefore, the surface wettability of IL-MoO_3 is relevant for applications such as sensors and biosensors.

Figure 4. *Wetabillity test of IL-MoO_3*

Particle size distribution and zeta potential

Dynamic light scattering (DLS) analysis was performed for further assessment of particle size distribution. Figure 5(a) shows the particle size distribution of IL-MoO_3 nanoparticles investigated by the laser diffraction method and DLS technique. The obtained results revealed that the particle size distribution of IL-MoO_3 ranges from 20 to 150 nm with the mean particle size of 65 nm. This suggests a broad distribution range of oxide nanoparticles size, and gives the average particle size of IL-MoO_3.

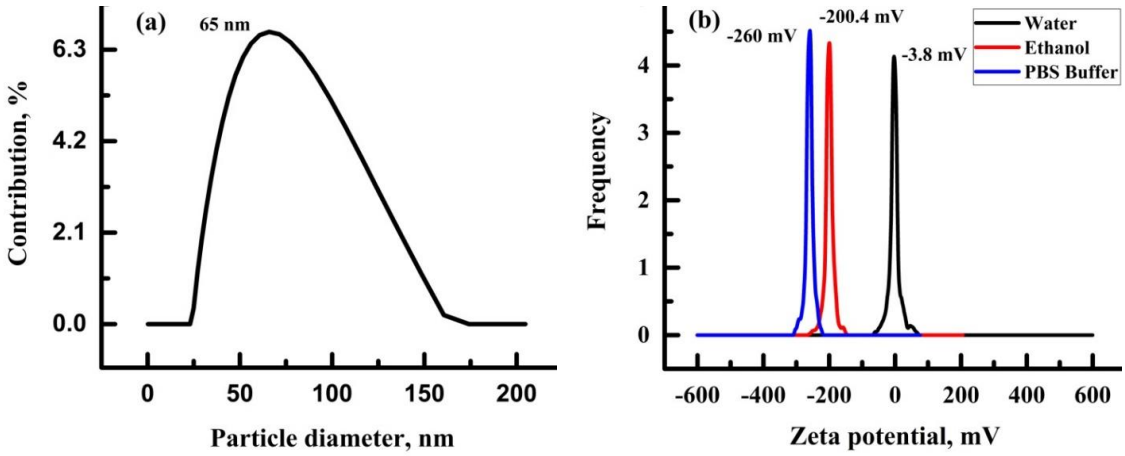

Figure 5. *(a) Particle size distribution vs. particle diameter and (b) zeta potential of IL-MoO_3 in various solvent systems*

Figure 5(b) depicts zeta potential in different solvent systems, which is indicative for stability of IL-MoO_3. As shown in Figure 5(b), IL-MoO_3 nanoparticles possess high stability in the phosphate buffer solution (PBS) with the highest negative zeta potential of -260 mV, as compared to -202 mV for ethanol. The lowest stability is observed in water (-3.8 mV). These results suggest that the pre-

sence of IL increases stability of MoO_3, possibly due to electrostatic interactions of IL and MoO_3 [39]. Agglomeration of IL-MoO_3 in the water system leads to low stability of dispersion, what is one of the factors for the observed low zeta potential magnitude of -3.8 mV.

Electroanalysis of 4-NP at modified electrode

CV and DPV techniques were employed to investigate the electrochemical behavior of 4-NP at the surface of IL-MoO_3/GCE. Figure 6(a) shows cyclic voltammograms of blank phosphate buffer solution (pH 5.8), and the same solution containing 37 μM 4-NP. No faradic activity at IL-MoO_3/GCE occurred in the blank solution, but the current was increased significantly when phosphate buffer solution contained 37 μM of 4-NP. Three distinct anodic and cathodic current peaks can be observed, where the first redox pair (Ox_1/Red_1) is associated with E_{pa} at 0.05 V, and E_{pc} at 0.008 V, with peak separation of 42 mV. The second redox pair (Ox_2/Red_2) shows the oxidation peak at 0.27 V, and reduction peak at 0.18 V, with peak separation of 90 mV, while the third redox pair (Ox_3/Red_3) is associated with E_{pa} at 0.49 V, and E_{pc} at 0.36 V, with 130 mV peak to peak separation.

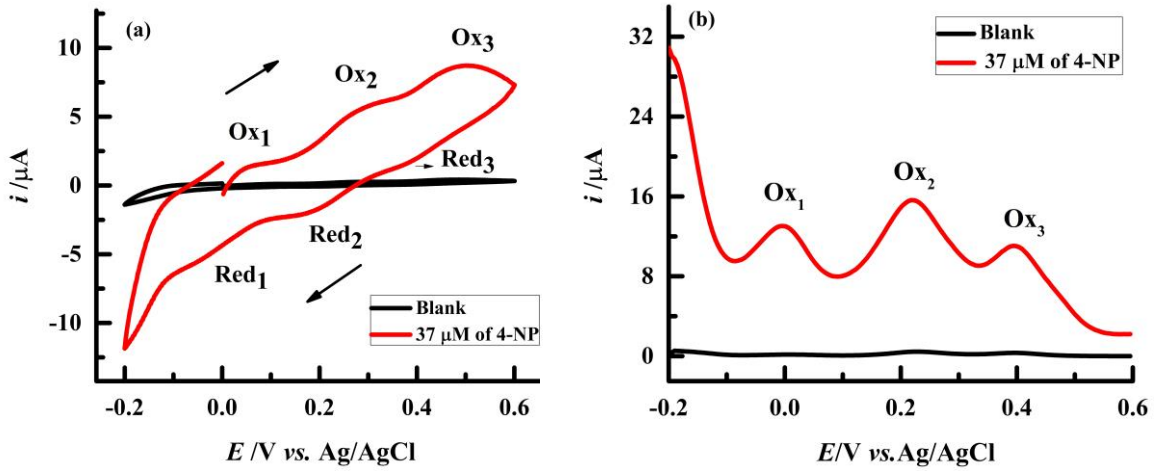

Figure 6. *Voltammetric responses of IL-MoO_3/GCE in phosphate buffer solution (pH 5.8) without (blank) or with 37 μM 4-NP recorded at 50 mV/s by (a) CV and (b) DPV*

Similarly, DPVs shown in Figure 6(b) also reveal poor faradic current response at IL-MoO_3/GCE in the blank solution, and considerable enhancement of faradic current in the presence of 37 μM of 4-NP. Well-defined anodic potentials (E_{Ox_1}= 0.06 V, E_{Ox_2} = 0.27 V and E_{Ox_3} =0.4 V) of three redox peaks can be noticed in DPV of IL-MoO_3/GCE in phosphate buffer solution (pH 5.8) contining 4-NP. Such strong enhancement of CV and DPV current values, suggests higher electrocatalytic activity of IL-MoO_3 modified GCE towards 4-NP. This can be attributed to larger surface area and bonding between Mo-O of IL-MoO_3 which facilitates the electron transfer significantly. Moreover, the effective interaction between IL and metal oxide nanoparticles can promote the electro-catalytic activity of 4-NP [40]. Therefore, IL-MoO_3 manifests excellent properties for electrochemical sensing of 4-NP. According to literature, organic molecules usually undergo multiple electron transfer reaction with successive steps and formation of intermediates. In such multi-electron transfer, CV consists of distinct redox peaks and waves that are well separated.

Interaction of IL-MoO_3 and 4-NP

CV scanning in the positive direction (-0.2 to 0.6 V) induces oxidation of 4-NP, and as a result, MoO_3(VI) gets reduced to Mo(V) in the form of MoO_2(OH), due to chemisorbed (OH^-) anions at the interfacial electrode surface [41-43]. Therefore, superior interaction between chemisorbed OH^- and π

effect of 4-NP enhances oxidation of 4-NP. When CV was scanned in the reverse direction toward negative potentials, the negative charge gets collected at the surface region of IL-MoO_3/GCE, which increased reduction of 4-NP. This is due to the availability of adsorption sites on the surface of IL-MoO_3 which shows high electro-catalytic effect of 4-NP.

Effect of varying concentration of 4-NP

Sensing performance of IL-MoO_3/GCE was studied by cyclic voltammetry with diverse concentrations of 4-NP (7.48 - 73.1 μM). Figure 7(a) reveals that peak currents increased with increase of the concentration of 4-NP. Figure 7(b) depicts linear relation between anodic peak current of Ox_3 and concentration of 4-NP within a wide linear range (7.48 to 73.1 μM). The linear regression equation was defined as: $i_p = 2\times10^{-6} + 0.106C$ (R^2=0.99). The detection limit (LOD) and quantification limit (LOQ) were calculated using following equations:

$$LOD = 2S_b / K \quad (7)$$

$$LOQ = 10S_b / K \quad (8)$$

where, S_b is standard deviation and K is slope of the calibration plot [29]. LOD and LOQ values were determined as 6.76 and 22.5 μM, respectively.

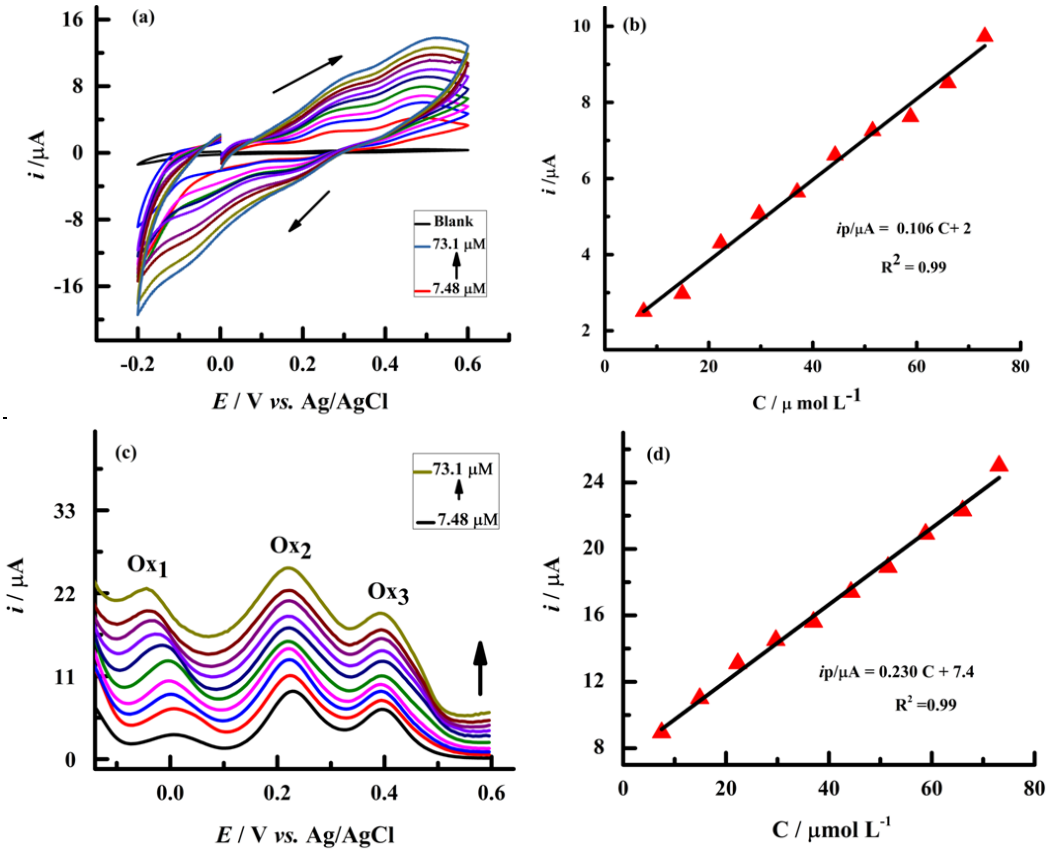

Figure 7. *Effect of increasing concentration of 4-NP (7.48-73.1μM) in phosphate buffer solution (pH 5.8) on voltametric response of IL-MoO_3/GCE, recorded by (a) CV at 50 mV/s; b) linear variation of Ox_3 peak current against concentration; (c) DPV at 50 mV/s; (d) linear variation of Ox_2 peak current against concentration*

Similarly, Figure 7(c) shows DPV responses of 4-NP in the concentration range from 7.48 to 73.1 μM. Three diverse oxidation peaks can be observed (ascribed as Ox_1, Ox_2 and Ox_3), which all increase with increase of the concentration of 4-NP. This suggests that IL-MoO_3/GCE exhibits higher catalytic activity at higher concentrations of 4-NP. The highest peak current was observed for Ox_2 and selected for construction of the calibration plot shown in Figure 7(d). The calibration plot

depicted in Figure 7(d) shows linearity between peak current and concentration of 4-NP, and linear regression was found to be: $i_p = 7.42\times10^{-6} + 0.230C$ (R^2=0.99) LOD and LOQ determined from DPV were calculated as 5.41 and 18.0 μM, respectively. Furthermore, the sensitivity of IL-MoO_3/GCE was calculated using the following equation:

$$\text{Sensitivity} = m / A \quad (9)$$

where m is slope of calibration plot and A is active surface area [44]. The calculated sensitivity from CV and DPV was 0.212 and 0.461 A L mol^{-1} cm^{-2}, respectively.

Table 1 compares analytical performances (LOD and linear range of 4-NP) obtained for IL-MoO_3/GCE and some other modified electrodes using different voltametric techniques.

By comparing data listed in Table 1, it is clear that IL-MoO_3/GCE possesses comparable or even better analytical performances towards 4-NP determination than other modified electrodes [45-48].

Table 1. *Comparison of analytical performances of various modified electrodes for 4-NP determination using voltametric techniques*

Ser. No	Electrode	Method	Linear range of $C_{4\text{-NP}}$, μM	LOD, μM	Reference
1	GNS-FePc/GCE	CV	100 -700	10.00	[45]
2	ZG-2/GCE, ZnO/GCE	CV	10 -1000	13.00	[46]
3	Nano-Au /GCE	LSV	10 -1000	8.00	[47]
4	Pt/inorganic organic coatings	SWV	30–90	10.28	[48]
5	CNT/SPE	DPV	25 – 620	1.3	[49]
6	Pd-GA/RGO	CV	2-80	9×10^{-9}	[50]
7	rGO–HNT–AgNPs	CV	0.1 - 363.9	0.0486	[51]
8	MoS_2/GCE	DPV	4-0.02	0.01	[52]
9	IL-MoO_3/GCE	CV	7.48 - 73.1	6.76	Present work
10	IL-MoO_3/GCE	DPV	7.48 - 73.1	5.41	Present work

GNS-FePc- graphene nanosheets decorated iron phthalocyanine; ZG-zinc glycerolate nano-gel, CNT- carbon nanotubes, SPE- screen printed electrode; Pd-GA/RGO - Pd nanospheres decorated reduced graphene oxide; rGO–HNT–AgNPs- reduced graphene oxide-halloysite nanotubes-silver nanoparticles.

Among modified electrodes reported in Table 1, there are few carbon-based electrodes (CNT and GNS) [45,49], which are generally considered as superior candidates for electrochemical sensing due to high surface area and wide potential window. However, the major drawback of the carbon-based sensor is necessity for its purification and synthetic protocol which may affect sensitivity of analyte. In comparison to electrodes modified by noble metals, as well as carbon nanotubes modified electrodes that were already tested for determination of 4-NP [45,50], here developed IL-MoO_3/GCE system is inexpensive and Hg-free material, that can be applied in rather uncomplicated and facile detection method. The linear dynamic range and limit of detection are found within the biological range of 4-NP, what is a prominent advantage of the present method.

Table 2 represents the results of comparison of LOD values for 4-NP determination obtained in this work and by some usual (not electrochemical) analytical methods.

Table 2. *Comparison of LOD values for some analytical methods used for 4-NP determination*

Analytical method	LOD, μM	Reference
Colorimetry	6.30	[53]
HPLC	0.021	[54]
Fluorometry	0.2	[55]
Colorimetry	1.28	[56]
Spectrophotometry	0.057	[57]
CV	6.76	This work
DPV	5.41	This work

From data in Table 2, it is clear that electrochemical sensing techniques used in the present work show moderate sensitivity compared to other, but rather expensive analytical methods. It seems, however, that a flower shape MoO_3 possesses significant catalytic activity towards 4-NP. Therefore, it could be expected that by varying synthesis parameters such as temperature and time, a diverse morphology of IL-MoO_3 could be obtained, resulting eventually in even better catalytic response towards 4-NP. Generally, this work represents the facile synthetic strategy of MoO_3 that could be a basis for its further development and application in the electrochemical analysis of other potential organic pollutants.

Effect of varying scan rate

Influence of the scan rate on 4-NP redox peaks was also examined within the scan rate range of 10-100 mV/s. It can be seen in Figure 8(a) that all redox peak currents increase with increasing scan rate.

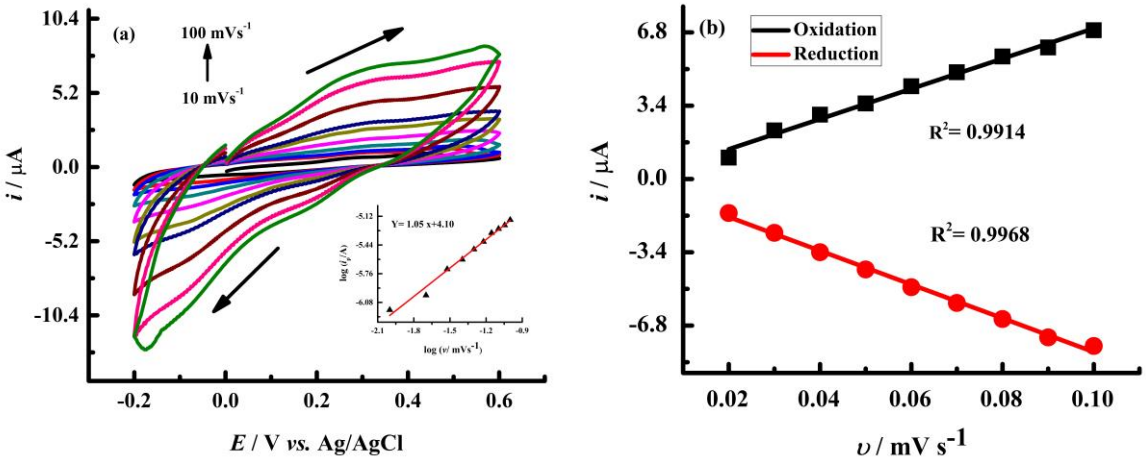

Figure 8. *(a) Effect of increasing scan rate (10-100 mV/s) on CV of IL-MoO_3/GCE in phosphate buffer solution (pH 5.8) containing 73.1 µM of 4-NP. Inset: log of anodic peak (Ox_1) current vs. log of scan rate; (b) anodic (oxidation) and cathodic (reduction) peak currents (Ox_1/Red_1) vs. scan rate*

Figure 8(b) represents linear correlations of anodic and cathodic peak currents (Ox_1/Red_1) with respect to the scan rate. Linear regression equations were found out as: i_{pa} (µA) = 70 + 0.09 (R^2 = 0.9914), and i_{pc} (µA) = - 80 – 0.2 (R^2=0.9968).

Good linearity between peak current and scan rate suggests that surface adsorption process of 4-NP is occurring at IL-MoO_3/GCE surface [58]. Furthermore, the inset of Figure 8(a) shows the linear plot of log peak current versus log scan rate, with the slope value 1, indicating adsorption-controlled process [58-59]. This confirms that adsorption of 4-NP is energetically favorable at IL-MoO_3/GCE. The amount of adsorbed 4-NP at IL-MoO_3/GCE was calculated as 7.80×10^{-11} mol cm^{-2} using the following formula [60]:

$$\Gamma = Q / nFA \quad (10)$$

where, Γ is amount of adsorbed analyte in mol cm^{-2}, n is the number of transferred electrons, Q is total charge, F is Faraday's constant, and A is surface area of electrode in cm^2. The relatively high amount of adsorbed 4-NP signifies high surface area possessed by IL-MoO_3/GCE.

Effect of pH

The impact of pH of phosphate buffer solution on the electrode reaction of 73.1 µM of 4-NP was recorded at pH 5.8, 7.4 and 8.3 (acidic, neutral and basic media) at the favored scan rate of 50 mVs^{-1}. Figure 9(a) depicts no faradic activity at pH 8.3, but slightly increased currents are observed at pH 7.4.

Drastic enhancement of faradic current, however, was observed in pH 5.8, what implies that redox behavior of 4-NP is pH dependent. Figure 9(b) shows the relationship between peak current and pH, in which the utmost current peak is reached at pH 5.8. This indicates that the protic environment of the solution promotes the electron transfer process over the surface of the electrode [60].

In a highly alkaline medium, the electrostatic repulsion between 4-NP anions and hydroxyl groups significantly increases, and as a result, the barrier to remove 4-NP is increased. Therefore, 4-NP becomes less reactive in the basic buffer system, while in the acidic media degradation of 4-NP is feasible. Figure 9(c) represents that the anodic peak potential (E_{pa}) is linearly decreased as pH was increased from 5.8 to 8.3. The corresponding linear regression equation was found out to be: E_{pa} = - 0.47 pH + 0.61 (R^2=0.99). The slope obtained from this equation is nearly equal to the Nernstian value of 58.5 mV/pH, signifying that the electrochemical reaction of 4-NP carries equal number of protons and electrons [60], *i.e.*, two electrons and two protons in the present case. Also, from the negative slope, it is clear that the electron transfer process is facilitated by protonation. Hence from the above experimental observations pH 5.8 was opted out for further analysis.

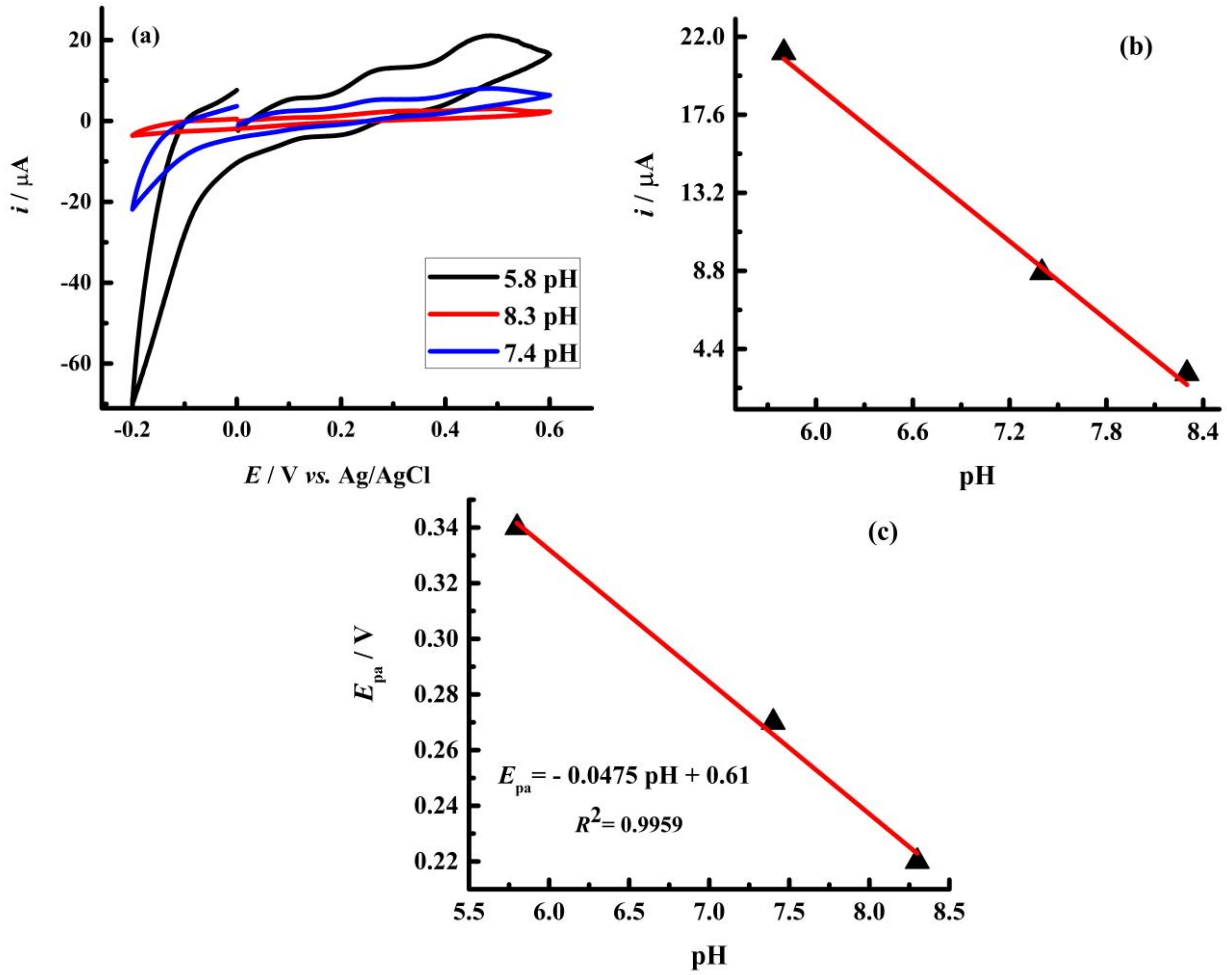

***Figure 9**. (a) CVs (50 mV/s) of IL-MoO_3/GCE in phosphate buffer solution containing 73.1 µM 4-NP at different pH (5.8-8.3); (b) oxidation peak current* vs. *pH; (c) oxidation peak potential* (E_{pa}) vs. *pH*

Electrochemical impedance spectroscopy (EIS)

EIS is an efficient tool to monitor kinetic and interfacial properties of modified electrodes. Curves (a) and (b) in Figure 10 represent Nyquist plots of bare GCE and IL-MoO_3/GCE in 0.1M KCl solution containing ferrocene redox probe. The frequency range varied from 10^5 to 0.1 Hz, and AC amplitude of 10 mV was applied to the system**.** The working potential of EIS measurements was 0.15 V.

Nyquist plots in Figure 10 show that both electrodes exhibit semicircular parts in high-frequency region, followed by straight lines at lower frequencies. This is characteristic electrode impedance response when electron transfer kinetics is controlled by diffusion process. It is also well known in impedance data analysis that the diameter of semicircular part in a Nyquist plot denotes charge transfer resistance (R_{ct}) of redox reaction, while straight line of about -π/4 slope denotes diffusion impedance (W) of reaction species (ferrocene here).

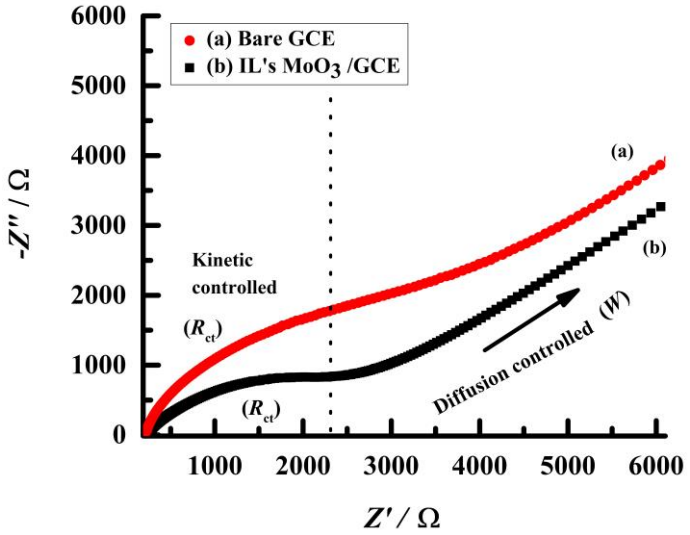

Figure 10. *Nyquist plots of bare GCE and IL-MoO_3/GCE in 0.1 M KCl and 1 mM ferrocene*

According to Figure 10, bare GCE showed higher semicircular part, indicating a higher R_{ct} value (78.7 Ω) than IL-MoO_3/GCE (38.6 Ω). This suggests that bare GCE possesses higher resistance to the electron transfer, while IL-MoO_3/GCE shows smaller resistance to electron transfer at the electrode interface. The apparent electron transfer rate constant k_{app} was calculated using the equation (11) [61]:

$$k_{app} = \frac{RT}{n^2F^2R_{ct}AC} \quad (11)$$

where R_{ct} is charge transfer resistance, C is concentration of redox probe (1 mM ferrocene), n = 1 is the number of transferred electrons, A is electrode surface area, while R, T and F have their usual meaning. The values of k_{app} and R_{ct} are given in Table 3. Increase of k_{app} values and decrease of R_{ct} values when compared to bare GCE imply an improvement of electron transfer at IL-MoO_3/GCE, suggesting its increased activity toward redox reaction.

Table 3. *Charge transfer resistance (R_{ct}) and k_{app} values for bare GCE and IL-MoO_3/GCE in 0.1 M KCl and 1 mM ferrocene*

Electrode	R_{ct} / Ω	k_{app} / 10^3 cm s^{-1}
Bare GCE	78.7	6.26
IL–MoO_3/GCE	36.8	13.4

Reproducibility and stability

Reproducibility was investigated by repetitive measurements using different IL-MoO_3/GCE to estimate the sensing performance of 73.1 mM of 4-NP in favorable conditions. The obtained RSD value was less than 2 %, suggesting superior reproducibility of the designed sensor. Stability of the modified electrode was tested for successive 25 cycles. Before analysis, the electrode was kept in a dry condition for 30 days. The percentage degradation was calculated using Eq. (12) [62, 63]

Degradation, % = (i_{pl} / i_{pi}) 100 (12)

where, i_{pl} and i_{pi} denote last and initial anodic peak current, respectively. The calculated degradation was 94 %, what indicates that IL-MoO_3/GCE shows satisfactory reproducibility and stability.

Interference study

Figure 11 shows selectivity property of the modified sensor. It was evaluated using CV by inspecting the effect of possible interferents such as aniline and resorcinol (20 µM of each) in 0.2 M phosphate buffer solution (pH 5.8) containing 20 µM 4-NP. Since, aniline and resorcinol along with 4-NP are commonly used as starting materials in various industries, just these two organic pollutants in combination with 4-NP were selected for the interference study at IL-MoO_3/GCE. It is obvious from Figure 11, that the redox peaks around 0.26 V and 0.48 which were used for the determination of 4-NP remained unaffected as 20 µM aniline and resorcinol were added. In fact, no redox activity was observed for aniline and resorcinol looking separately. This result suggests that the designed sensor exhibit outstanding selectivity towards 4-NP.

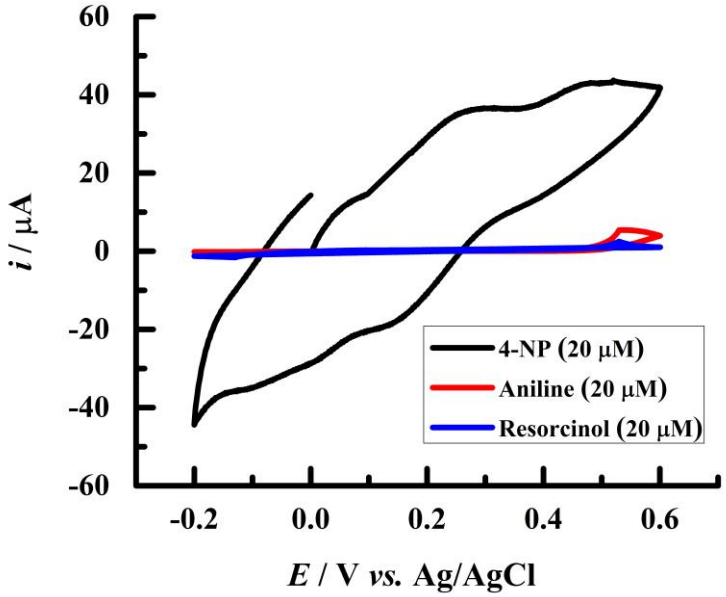

Figure 11. *Interference study of 4-NP with aniline and resorcinol*

Application of IL-MoO_3/GCE in real water samples

Determination of 4-NP in water samples from Krishna and Panchganga rivers using IL-MoO_3/GCE was performed, and results are shown in Table 4. A recovery study was carried out using the standard addition method. Finally, differential pulse voltammogram was recorded, showing a clear signal of 4-NP oxidation. The recovery percentage was calculated using Eq. (13) [29]:

$$\text{Recovery, \%} = (C_{4\text{-NP}} \text{ found} / C_{4\text{-NP}} \text{ added}) \, 100 \quad (13)$$

The recovery was nearly 100 and 98 %, respectively, which indicates that IL-MoO_3 modified GCE sensor has good efficiency and sensitivity for 4-NP determination.

Table 4. *Determination of 4-NP in river water samples*

Sample	Amount of 4-NP, µM		Recovery, %
	Added amount of 4- NP	Found amount of 4-NP	
1	14.5	14.5	100
2	15.3	15.0	98.0
3	16.6	16.3	98.1
Standard deviation		0.092	

Conclusions

Within green approach toward the synthesis of metal oxide nanomaterials, ionic liquid $[BMIM]^+[Br]^-$ was utilized for the successful synthesis of MoO_3. The obtained thin film was dispersed in ethanol and IL-MoO_3 nanoparticles were subsequently used to modify GCE surface. The modified electrode, IL-MoO_3/GCE, was tested as a sensor for the important organic pollutant, 4-NP, Promising results were obtained, showing IL-MoO_3/GCE as the efficient sensor for determination of 4-NP. The limit of detection (LOD) values estimated from CV and DPV as 5.41 and 6.76 μM were found close or even better than for some other modified electrodes taken from the literature. The calculated sensitivity from CV and DPV was 0.212 and 0.461 A L mol^{-1} cm^{-2}, respectively, suggesting that the fabricated sensor exhibits excellent sensitivity towards 4-NP. In addition, the developed sensor manifested high selectivity, by showing no considerable interference with some foreign organic pollutants (aniline and resorcinol). IL-MoO_3/GCE was successfully applied for determination of 4-NP in river water samples, and the obtained results indicate that modified electrode can be utilized to monitor other environmental pollutants in sustainable way for the healthy environment.

References

[1] K. Yoshida, T. Shigeoka, F. Yamauchi, *Ecotoxicology and Environmental Safety* **7(2)** (1983) 179-190. https://doi.org/10.1016/0147-6513(83)90064-7

[2] K. Hustert, M. Mansour, H. Parlar, F. Korte, *Chemosphere* **10(9)** (1981) 995-998. https://doi.org/10.1016/0045-6535(81)90200-9

[3] G. Eichenbaum, M. Johnson, D. Kirkland, P. O'Neill, S. Stellar, J. Bielawne, R. DeWire, D. Areia, S. Bryant, S. Weiner, D. Desai-Krieger, P. Guzzie-Peck, D.C. Evans, A. Tonelli, *Regulatory Toxicology and Pharmacology* **55(1)** (2009) 33-42. https://doi.org/10.1016/j.yrtph.2009.05.018

[4] S. V. Kite, D. J. Sathe, A. N. Kadam, S. S. Chavan, K. M. Garadkar, *Research on Chemical Intermediates* **46(2)** (2020) 1255-1282. https://doi.org/10.1007/s11164-019-04032-7

[5] Z. Dong, X. Le, C Dong, W. Zhang, X. Li, J. Ma, *Applied Catalysis B: Environmental* **162** (2015) 372-380. https://doi.org/10.1016/j.apcatb.2014.07.009

[6] J. Karaová, J. Barek, K. Schwarzová-Pecková, *Analytical Letters* **49** (2016) 66-79. https://doi.org/10.1080/00032719.2014.1003424

[7] C. Borrás, T. Laredo, J. Mostany, B. R. Scharifker, *Electrochimica Acta* **49(14)** (2004) 641-648. https://doi.org/10.1016/j.electacta.2003.09.019

[8] X. Guo, Z. Wang, S. Zhou, *Talanta* **64(1)** (2004) 135-139. https://doi.org/10.1016/j.talanta.2004.01.020

[9] H. R. Sobhi, A.Esrafili, H. Farahani, M. Gholami, M. M. Baneshi, *Environmental Monitoring and Assessment* **185** (2013) 9055-9065. https://doi.org/10.1007/s10661-013-3235-y

[10] J. I. Cacho, N. Campillo, P. Viñas, M. Hernández-Córdoba, *Journal of Chromatography A* **1241** (2012) 21-27. https://doi.org/10.1016/j.chroma.2012.04.018

[11] M. Christwardana, Y. Chung, D. C. Tannia, Y. Kwon, *Korean Journal of Chemical Engineering* **35** (2018) 2421-2429. https://doi.org/10.1007/s11814-018-0163-0

[12] Nambudumada S. Prinith, J. G. Manjunatha, *Journal of Electrochemical Science and Engineering* **10(4)** (2020) 305-315. https://doi.org/10.5599/jese.774

[13] Z. Liu, J. Du, C. Qiu, L. Huang, H. Ma, D. Shen, Y. Ding, *Electrochemistry Communication* **11(7)** (2009) 1365-1368. https://doi.org/10.1016/j.elecom.2009.05.004

[14] Z. Liu, H. Zhang, H. Ma, S. Hou, *Electroanalysis* **23** (2011) 2851-2861. https://doi.org/10.1002/elan.201100385

[15] Y. E Gu, Y. Zhang, F. Zhang, J. Wei, C. Wang, Y. Du, W. Ye, *Electrochimica Acta* **56(2)** (2010) 953-958. https://doi.org/10.1016/j.electacta.2010.09.051

[16] J. Li, D. Kuang, Y. Feng, F. Zhang, Z. Xu, M. Liu, *Journal of Hazardous Materials* **(201-202)** (2012) 250-259. https://doi.org/10.1016/j.jhazmat.2011.11.076

[17] X. Jiao, H. Luo, N. Li, *Journal of Electroanalytical Chemistry* **691** (2013) 83-89. https://doi.org/10.1016/j.jelechem.2012.12.013

[18] M. Danish, A. Bhattacharya, D. Stepanova, A. Mikhaylov, M. L. Grilli, M. Khosravy , T. Senjyu, *Metals* **10** (2020) 1604. https://doi.org/10.3390/met10121604
[19] N. Guru Prakash, M. Dhananjaya, A. Lakshmi Narayana, Hussen Maseed, V. V. S. S. Srikanth, O. M. Hussain, *Applied Physics A* **125** (2019) 488. https://doi.org/10.1007/s00339-019-2779-2
[20] K. Inzani. T. Grande, F. Vullum-Bruer, S. M. Selbach, *The Journal of Physical Chemistry C* **120(16)** (2016) 8959-8968. https://doi.org/10.1021/acs.jpcc.6b00585
[21] N. Tahmasebi, M. Khalildashti, *Korean Journal of Chemical Engineering* **37** (2020) 448-455. https://doi.org/10.1007/s11814-019-0469-6
[22] I. Shaheen, K. S. Ahmad, C. Zequine, R. K. Gupta, A. G. Thomas, M. A. Malik, *Journal of Energy Storage* **29** (2020) 101309. https://doi.org/10.1016/j.est.2020.101309
[23] A. Dhara, G. Hodes, S. K. Sarkar, *RCS Advances* **4** (2014) 53694-53700. https://doi.org/10.1039/C4RA08606F
[24] G.R Mutta, S.R Popuri, J.I.B. Wilson, N.S. Bennett, *Solid State Sciences* **61** (2016) 84-88. https://doi.org/10.1016/j.solidstatesciences.2016.08.016
[25] J. Gong, W. Zeng, H. Zhang, *Materials Letters* **154** (2015) 170-172. http://dx.doi.org/10.1016/j.matlet.2015.04.092
[26] N. Karousis, T. Ichihashi, S. Chen, H. Shinohara, M. Yudasaka, S. Iijima, N. Tagmatarchis, *Journal of Materials Chemistry* **20** (2010) 2959-2964. https://doi.org/10.1039/B925169C
[27] Y. Cheng, Z. Chen, H. Wu, M. Zhu, Y. Lu, *Advanced Functional Materials* **26** (2016) 1338-1346. https://doi.org/10.1002/adfm.201504134
[28] B. B. Kamble, B. D. Ajalkar, A. K.Tawade, K. K. Sharma S. S. Mali, C. K. Hong, C. Bathula, A. N. Kadam, S. N.Tayade, *Journal of Molecular Liquids* **324** (2021) 115119. https://doi.org/10.1016/j.molliq.2020.115119
[29] A. A. A. Aljabali, J. E. Barclay, J.N. Brett, G. P. Lomonossoff, D.J. Evans, *Dalton Transactions* **39** (2010) 7569-7574. https://doi.org/10.1039/C0DT00495B
[30] A. Boukhachem, M. Mokhtari, N. Benameur, A. Ziouche, M. Martínez, P. Petkova, M. Ghamnia, A. Cobo, M. Zergoug, M. Amlouk, *Sensors and Actuators A: Physical* **253** (2017) 198-209. https://doi.org/10.1016/j.sna.2016.11.032
[31] M. Sasidharan, N. Gunawardhana, H. Noma, M. Yoshio, K. Nakashima, *Bulletin of the Chemical Society of Japan* **85(5)** (2012) 642-646. https://doi.org/10.1246/bcsj.20110375.
[32] D. Chen, M. Liu, L. Yin, T. Li, Z. Yang, X. Li, B. Fan, H. Wang, R. Zhang, Z. Li, H. Xu, H. Lu, D. Yang, J. Sun, L. Gao, *Journal of Materials Chemistry* **21** (2011) 9332-9342. https://doi.org/10.1039/C1JM11447F
[33] T. Rajkumar, G. R. Rao, *Journal of Chemical Sciences* **120** (2008) 587-594. https://doi.org/10.1007/s12039-008-0089-x
[34] J. Bowers, C. P. Butts, P. J. Martin, M. C. Vergara-Gutierrez, R. K. Heenan, *Langmuir* **20(6)** (2004) 2191-2198. https://doi.org/10.1021/la0359 40m.
[35] X. Duan, T. Kim, D. Li, J. Ma, W. Zheng, *Chemistry-A European Journal* **19** (2013) 5924-5937 https://doi.org/10.1002/chem.201203176
[36] A. Moldovan, M. Enachescu, *Wetting properties at nanometer scale*, IntechOpen, 2015. DOI: 10.5772/60886.
[37] P. Kanyong, S. Rawlinson, J. Davis, *Sensors and Actuators B: Chemical* **233** (2016) 528-534. https://doi.org/10.1016/j.snb.2016.04.099
[38] M. Irfan, T. Ahmad, M. Moniruzzaman, S. Bhattacharjee, B. B. Abdullah, *Arabian Journal of Chemistry* **13(1)** (2017) 75-85. http://dx.doi.org/10.1016/j.arabjc.2017.02.001
[39] M.-A. Neouze, *Journal of Materials Chemistry* **20** (2010) 9593-9607. https://doi.org/10.1039/C0JM00616E
[40] M. W. Hsiao, R. R. Adžić, E. B. Yeager, *Journal of the Electrochemical Society* **143(3)** (1996) 759-767. https://doi.org/10.1149/1.1836536
[41] G. Kokkinidis, J. M. Leger, C. Lamy, *Journal of Electroanalytical Chemistry and Interfacial Electrochemistry* **242(1-2)** (1988) 221-242. https://doi.org/10.1016/0022-0728(88)80253-5
[42] Y. Kim, K. Giribabu, J. G. Kim, J. B. Lee, W. G. Hong, Y. S. Huh, H. J. Kim, *ACS Sustainable Chemistry Engineering* **7(4)** (2019) 4049-4102. https://doi.org/10.1021/acssuschemeng.8b05603

[43] M. M. Rahman, *Microchemical Journal* **157** (2020) 104945. https://doi.org/10.1016/j.microc.2020.104945
[44] R. Devasenathipathy, V. Mani, S. M. Chen, K. Manibalan, S. T. Huang, *International Journal of Electrochemical Science* **10** (2015) 1384-1392.
[45] A. Sinhamahapatra, D. Bhattacharjya, J.-S. Yu, *RSC Advances* **5** (2015) 37721-37728. https://doi.org/10.1039/C5RA06286A
[46] L. Chu, L. Han, X. Zhang, *Journal of Applied Electrochemistry* **41(6)** (2011) 687-694. https://doi.org/10.1007/s10800-011-0281-4
[47] T. Lupua, C. Lete, M. Marin, N. Totir, P. C. Balaure, *Electrochimica Acta* **54(7)** (2009) 1932-1938. https://doi.org/10.1016/j.electacta.2008.07.051
[48] A. Arvinte, M. Mahosenaho, M. Pinteala, A.-M. Sesay, V. Virtanen, *Microchimica Acta* **174** (2011) 337-343. https://doi.org/10.1007/s00604-011-0628-x
[49] A. T. E. Vilian, S.R. Choe, K. Giribabu, S. C. Jang, C. Roh, Y. S. Huh, Y.-K. Han, *Journal of Hazardous Materials* **333** (2017) 54-62 https://doi.org/10.1016/j.jhazmat.2017.03.015.
[50] K.-Y. Hwa, T. S. K. Sharma, A. Ganguly, *Inorganic Chemistry Frontiers* **7** (2020) 1981-1994. https://doi.org/10.1039/D0QI00006J
[51] T. Jeyapragasam, J. Meena Devi, V. Ganesh, *Ionics* **24** (2018) 4033-4041. https://doi.org/10.1007/s11581-018-2538-y
[52] S. Scarano, P. Palladino, E. Pascale, A. Brittoli, M. Minunni, *Microchimica Acta* **186** (2019) 146. https://doi.org/10.1007/s00604-019-3259-2
[53] S. Yaripour, A. Mohammadi, S. Mousavi, I. Esfanjani, N. Arabzadeh, S. Mozaffari, *Pharmaceutical Sciences* **25(1)** (2019) 57-64. https://doi.org/10.15171/PS.2019.9
[54] N. Xiao, S. G. Liu, S. Mo, N. Li, Y. J. Ju, Y. Ling, N. B. Li, H. Q. Luo, *Talanta* **184** (2018) 184-192. https://doi.org/10.1016/j.talanta.2018.02.114
[55] F. Qu, P. Chen, S. Y. Zhu, J. M. You, *Spectrochimica Acta Part A* **171** (2017) 449-453. https://doi.org/10.1016/j.saa.2016.08.043
[56] A. S. Miletić, E. T. Pecev-Marinković, Z. M. Grahovac, A. N. Pavlović, S. B. Tošić, I. D. Rašić Mišić, *Journal of Analytical Chemistry* **74** (2019) 521-527. https://doi.org/10.1134/S1061934819060066
[57] A. J. Bard, L. R. Faulkner, *Electrochemical Methods. Fundamentals and Applications*, 2nd ed., John Wiley and Sons, New York. 2001.
[58] D. K. Gosser, Jr., *Cyclic Voltammetry; Simulation and Analysis of Reaction Mechanisms*, VCH, New York, 1993.
[59] N. Hareesha, J. G. Manjunatha, *Journal of Electroanalytical Chemistry* **878** (2020) 114533. https://doi.org/10.1016/j.jelechem.2020.114533
[60] Q. He, Y. Tian, Y. Wu, J. Liu, G. Li, P. Deng, D. Chen, *Nanomaterials* **9(3)** (2019) 429. http://dx.doi.org/10.3390/nano9030429
[61] D. Nkosi, J. Pillay, K. I. Ozoemena, K. Nouneh, M. Oyama, *Physical Chemistry Chemical Physics* **12(3)** (2010) 604-613. https://doi.org/10.1039/B918754E
[62] N. Hareesha, J. G. Manjunatha, *Journal of the Iranian Chemical Society* **17** (2020) 1507-1519. https://doi.org/10.1007/s13738-020-01876-4
[63] M. M. Charithra, J. G. Manjunatha, *Journal of Electrochemical Science and Engineering* **10(1)** (2020) 29-40. http://dx.doi.org/10.5599/jese.717